

Nucleosome assembly is required for nuclear pore complex assembly in mouse zygotes

Azusa Inoue¹⁻⁴ & Yi Zhang¹⁻⁵

Packaging of DNA into nucleosomes not only helps to store genetic information but also creates diverse means for regulating DNA-templated processes. Attempts to reveal additional functions of the nucleosome have been unsuccessful, owing to cell lethality caused by nucleosome deletion. Taking advantage of the mammalian fertilization process, in which sperm DNA assembles into nucleosomes *de novo*, we generated nucleosome-depleted (ND) paternal pronuclei by depleting maternal histone H3.3 or its chaperone HIRA in mouse zygotes. We found that the ND pronucleus forms a nuclear envelope devoid of nuclear pore complexes (NPCs). Loss of NPCs is accompanied by defective localization of ELYS, a nucleoporin essential for NPC assembly, to the nuclear rim. Interestingly, tethering ELYS to the nuclear rim of the ND nucleus rescues NPC assembly. Our study thus demonstrates that nucleosome assembly is a prerequisite for NPC assembly during paternal pronuclear formation.

The nucleosome, composed of a core histone octamer wrapped by 147 bp of DNA, is the basic building block of chromatin¹. Assembly of genomic DNA into nucleosomes not only helps in storing genomic information but also creates diverse means for regulating DNA-templated processes such as transcription, replication and repair and aids in the compartmentalization of heterochromatin and euchromatin². In addition, nucleosomes serve as carriers of epigenetic information through post-translational modifications on histones and DNA^{3,4}. Although the functions of nucleosomes in the processes mentioned above are well documented, the biological consequences of genome-wide loss of nucleosomes in living eukaryotic cells are unknown.

Nucleosome depletion can be achieved through the depletion of core histones. However, it is difficult to realize this in higher eukaryotes because each of the core histones is encoded by multiple copies of genes⁵. In addition, histone-gene deletion results in immediate cell lethality⁶, thus preventing analysis of the effects of nucleosome depletion in living cells. An alternative that may allow depletion of nucleosomes is the inactivation of histone chaperones. However, functional redundancy between different histone chaperones renders this approach equally challenging⁷⁻⁹. Indeed, loss of histone H3.1 caused by depletion of the H3.1 chaperone CAF1 is compensated by histone H3.3 deposition by the H3.3-specific chaperone HIRA⁹. Similarly, although HIRA knockout impairs the enrichment of H3.3 within both active and repressed genes in cultured cells, nucleosome structures are not dramatically affected, owing to the presence of other histone variants and histone chaperones^{8,9}.

Throughout the life cycles of mammals and other animals, fertilization provides one of the best opportunities for understanding the biological function of nucleosome assembly, because nucleosome assembly occurs *de novo* after fertilization. The DNA in mature sperm

is primarily packaged by small and positively charged protamines instead of histones¹⁰. When a sperm enters an egg, the protamines are released, and maternal histones are incorporated into the sperm DNA to establish *de novo* nucleosomes^{11,12}. This naturally occurring process may provide a unique opportunity for generating a ND paternal pronucleus by blocking the *de novo* nucleosome assembly process.

Nucleosome assembly can take place in a replication-dependent or replication-independent manner. Whereas the canonical histones are deposited in a replication-dependent manner, the histone H3 variant H3.3 is deposited in a replication-independent manner^{13,14}. Previous studies have revealed that H3.3 is incorporated into mouse paternal DNA immediately after fertilization^{12,15,16} and that this is consistent with the localization of HIRA in the paternal chromatin in mouse zygotes¹². In addition, it has been shown that HIRA is responsible for H3.3 deposition on paternal DNA in *Drosophila*¹⁷. These observations suggest that HIRA is likely to have an important role in *de novo* nucleosome assembly in mouse paternal DNA after fertilization, although experimental evidence is lacking.

In this study, we set out to reveal additional functions of nucleosome assembly, and we generated ND paternal pronuclei in mouse zygotes through depletion of HIRA or H3.3. By investigating the consequence of genome-wide loss of nucleosomes, we revealed that nucleosome assembly is a prerequisite for functional nuclear-envelope (NE) formation and particularly for assembly of the NPC.

RESULTS

HIRA is required for H3.3 deposition in mouse zygotes

To examine whether HIRA is required for H3.3 deposition on mouse paternal DNA, we first analyzed the spatial and temporal relationships

¹Howard Hughes Medical Institute, Boston, Massachusetts, USA. ²Program in Cellular and Molecular Medicine, Boston Children's Hospital, Harvard Medical School, Boston, Massachusetts, USA. ³Division of Hematology/Oncology, Department of Pediatrics, Boston Children's Hospital, Boston, Massachusetts, USA. ⁴Department of Genetics, Harvard Medical School, Boston, Massachusetts, USA. ⁵Harvard Stem Cell Institute, Boston, Massachusetts, USA. Correspondence should be addressed to A.I. (az.usa.unc.hms@gmail.com) or Y.Z. (yzhang@genetics.med.harvard.edu).

Received 3 March; accepted 8 May; published online 8 June 2014; doi:10.1038/nsmb.2839

Figure 1 HIRA is required for H3.3 deposition on paternal DNA.

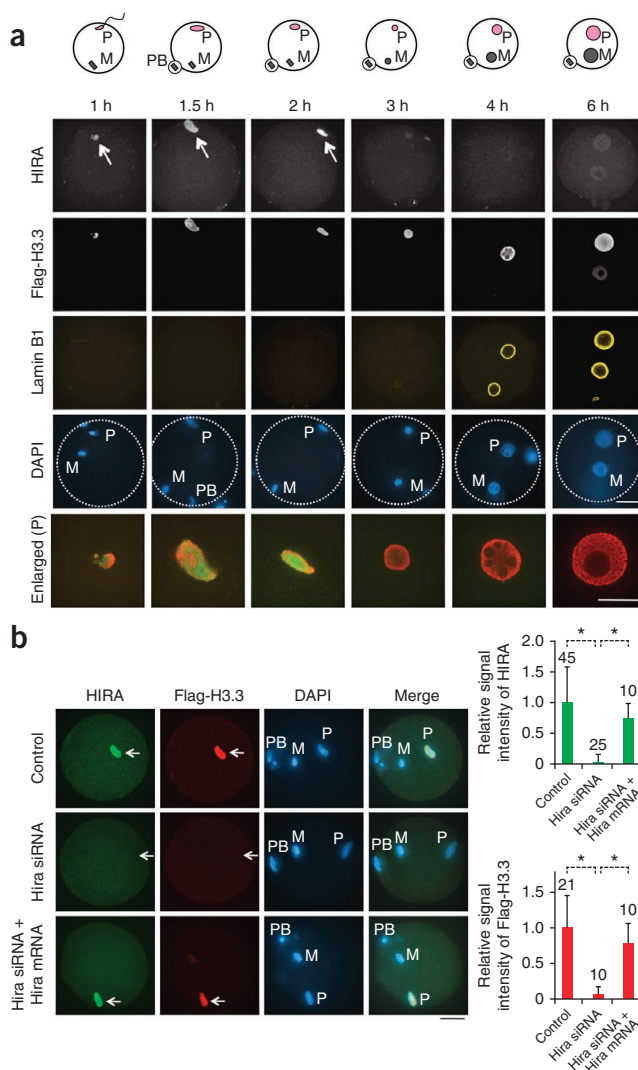
(a) Representative confocal microscopy images of fertilized mouse oocytes stained with anti-HIRA, anti-Flag and anti-lamin B1 (yellow) antibodies and DAPI (blue) at the indicated times post fertilization. The bottom row displays enlarged images of the paternal pronucleus with HIRA (green) and Flag-H3.3 (red) channels merged. A total of 11 (1 h), 7 (1.5 h), 19 (2 h), 20 (3 h), 13 (4 h) and 9 (6 h) zygotes were examined. Arrows indicate localization of HIRA to the paternal DNA. P, paternal DNA; M, maternal DNA, PB, polar body. Scale bar, 20 μ m. (b) Representative images of fertilized oocytes stained with anti-HIRA (green), anti-Flag (red) and DAPI (blue) at 2 h post fertilization (hpf). Arrows indicate the paternal DNA. Scale bar, 20 μ m. Graphs at right indicate relative values of the HIRA and Flag-H3.3 signal intensity in the paternal DNA. The value of control zygotes was set as 1.0. The numbers of zygotes examined in three independent experiments are indicated above the bars. * $P < 0.01$ by two-tailed Student's *t* test; error bars, s.d.

between HIRA localization and H3.3 deposition. Because an H3.3-specific antibody was not available, we injected Flag-H3.3 mRNA into metaphase II (MII)-stage oocytes and used an anti-Flag antibody to monitor the location of H3.3. Immunostaining revealed localization of HIRA exclusively to the paternal DNA at 1–2 h post fertilization (hpf), concomitantly with the deposition of Flag-H3.3 (Fig. 1a). After 3 hpf, the signal intensity of HIRA was greatly reduced, thus indicating that H3.3 deposition takes place immediately after fertilization and that the incorporated H3.3 is maintained thereafter. When the detection signal intensity was increased, we could detect HIRA signal in both pronuclei at 6 hpf, and this may account for the faint H3.3 signal in the maternal pronucleus. Lamin B1, a marker of the NE, was visible in both pronuclei at 4 hpf (Fig. 1a). Thus, the dynamics of HIRA and H3.3 is consistent with the potential role of HIRA in the asymmetric deposition of H3.3 in mouse zygotes.

To directly demonstrate a role of HIRA in H3.3 deposition, we attempted to deplete HIRA by injecting a Hira-specific short interfering RNA (siRNA) into germinal vesicle (GV)-stage oocytes. After meiotic maturation for 18 h, we fertilized the MII oocytes *in vitro* and fixed them at 2 hpf (Supplementary Fig. 1a). Despite a substantial reduction of Hira mRNA (Supplementary Fig. 1b), there was no significant reduction of HIRA protein (Supplementary Fig. 1c), thus indicating that HIRA protein is relatively stable and cannot be depleted by siRNA injection at GV stage.

To overcome this problem, we adopted a recently developed procedure (Supplementary Fig. 1d–f) in which siRNA is injected into small growing oocytes, and the injected oocytes are then cultured for 12 d to the fully grown GV stage (*in vitro* growth, IVG)¹⁸. This system is based on the idea that early destruction of target mRNAs can prevent accumulation of their protein products during oocyte growth and can lead to the depletion of stable maternal proteins. We first evaluated the quality of noninjected oocytes after IVG. After meiotic maturation following IVG (Supplementary Fig. 1g), 96% (94/98) of oocytes released the first polar body. After *in vitro* fertilization, 76% (67/88) of MII oocytes formed two pronuclei, and 78% (54/69) and 29% (20/69) of fertilized oocytes completed the first mitosis and developed to the blastocyst stage, respectively.

Using this system, we successfully depleted the HIRA protein in zygotes (Fig. 1b). Importantly, the deposition of Flag-H3.3 was prevented by HIRA depletion (Fig. 1b). The defective H3.3 deposition was caused by Hira knockdown, because H3.3 deposition was restored by co-injection of Hira mRNA that is resistant to Hira siRNA (Fig. 1b). Interestingly, protamines were undetectable in the paternal DNA of the control and the HIRA-depleted zygotes, but they were readily detectable in the unfertilized sperm (Supplementary Fig. 2), thus suggesting that protamine removal is independent of H3.3 incorporation.



Collectively, these results provide the first evidence, to our knowledge, demonstrating the functional conservation of HIRA in depositing H3.3 on paternal DNA in vertebrates.

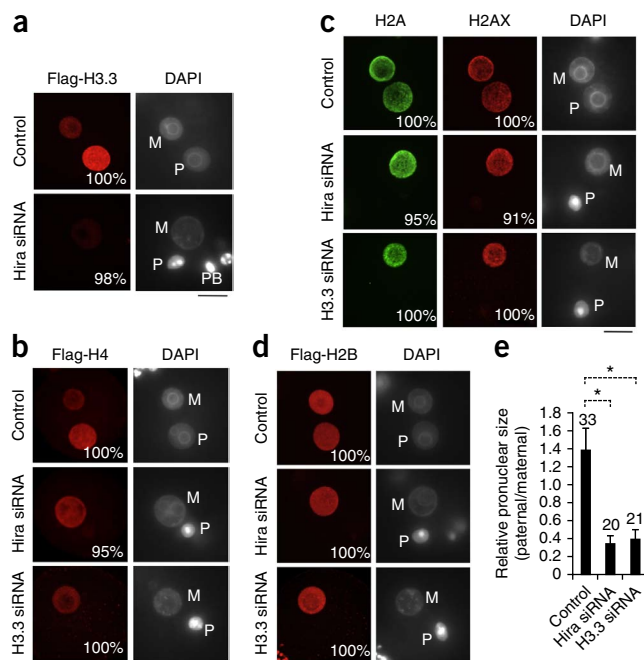
Loss of H3.3 deposition blocks *de novo* nucleosome assembly

To understand the role of H3.3 deposition, we examined the effect of defective H3.3 deposition on subsequent *de novo* nucleosome assembly of paternal DNA. Immunostaining at 8 hpf, a time corresponding to pronucleus stage 3 (PN3 stage), revealed that Flag-H3.3 still failed to accumulate in the paternal pronuclei (Fig. 2a). Interestingly, the paternal pronuclei of HIRA-depleted zygotes were much smaller than control pronuclei (Fig. 2a,e). Importantly, inhibition of H3.3 deposition also prevented the deposition of other core histones, including H4 (Fig. 2b), H2A and H2AX (Fig. 2c) and H2B (Fig. 2d), onto paternal DNA. This observation is in line with the deposition of H3–H4 tetramers preceding that of H2A–H2B dimers during nucleosome assembly *in vitro*¹⁹. In control-injected zygotes, in contrast to HIRA-depleted zygotes, all the core histones were properly deposited (Fig. 2b–d), in agreement with a previous report²⁰. These results demonstrate that *de novo* nucleosome assembly is prevented by HIRA depletion, and this allows the generation of ND paternal pronuclei.

To further confirm that the smaller paternal pronucleus is caused by lack of H3.3 deposition and not by other unknown functions associated with HIRA, we asked whether depletion of H3.3 results

Figure 2 *De novo* nucleosome assembly of paternal DNA is prevented by depletion of HIRA or H3.3. (a,b,d) Representative images of zygotes stained with anti-Flag antibody and DAPI at 8 hpf. Flag-H3.3 (a), Flag-H4 (b) or Flag-H2B (d) mRNA injected at GV stage are shown. The numbers of zygotes examined were 23 (control) and 41 (Hira siRNA) in a; 18 (control), 19 (Hira siRNA) and 11 (H3.3 siRNA) in b; and 16 (control), 33 (Hira siRNA) and 31 (H3.3 siRNA) in d. Percentages indicate zygotes showing the depicted phenotype. P, paternal DNA; M, maternal DNA; PB, polar body. Scale bars, 20 μ m. (c) Representative images of zygotes stained with anti-H2A (green) and anti-H2AX (red) antibodies and DAPI. A total of 18 (control), 22 (Hira siRNA) and 20 (H3.3 siRNA) zygotes were examined. Scale bar, 20 μ m. (e) Relative values of the area of pronuclei (paternal/maternal) are shown. The numbers of zygotes quantified in three independent experiments are indicated above the bars. * $P < 0.01$ by two-tailed Student's *t* test; error bars, s.d.

in similar defects. To deplete H3.3, we injected a mixture of siRNAs targeting H3.3A and H3.3B into GV oocytes. Analysis by reverse transcription and quantitative real-time PCR (RT-qPCR) confirmed that the mRNAs of both H3.3A and H3.3B, but not of Hira or other histones, were efficiently depleted (Supplementary Fig. 3a). After meiotic maturation and fertilization, we observed similar defects such as smaller paternal pronuclei and failure of histone incorporation (Fig. 2b–e). Notably, HIRA still localized to the paternal DNA in H3.3-depleted zygotes (Supplementary Fig. 3b), thus indicating that HIRA localization is independent of the presence of H3.3. The lack of nucleosome assembly in HIRA- or H3.3-depleted zygotes provided us with a unique opportunity to explore new functions of nucleosome assembly in the paternal pronucleus *in vivo*.

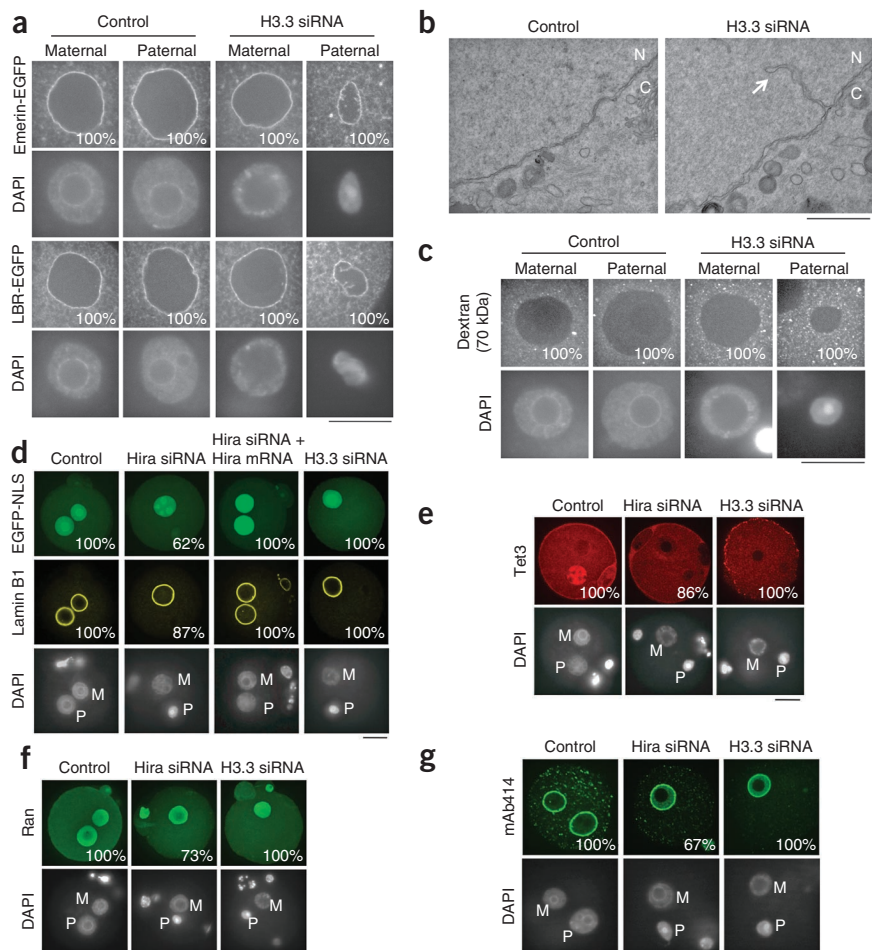


Nucleosome loss causes the formation of a NE devoid of NPCs

Nuclear expansion requires formation of the NE and protein nuclear transport^{21,22}. The smaller size of the ND paternal pronuclei (Fig. 2) raised the possibility that NE formation and/or protein nuclear transport might be impaired. To determine whether a NE is formed around

Figure 3 Nucleosome depletion causes the formation of NEs without NPCs.

(a) Representative images of the pronuclei of 8-hpf zygotes expressing emerin-EGFP or LBR-EGFP. A total of 9 and 27 zygotes (emerin-EGFP) and 13 and 33 zygotes (LBR-EGFP) for control and H3.3 siRNA, respectively, were examined. Percentages indicate zygotes showing the depicted phenotype. Scale bar, 20 μ m. (b) Representative TEM images of the paternal pronucleus at 8 hpf. Arrow indicates invagination of the inner nuclear membrane. N, nucleoplasm; C, cytoplasm. Scale bar, 1 μ m. (c) Representative images of the Dextran exclusion assay at 8 hpf. A total of 4 (control) and 12 (H3.3 siRNA) zygotes were examined. Scale bar, 20 μ m. (d) Representative images of zygotes expressing EGFP tagged with nuclear localization signal (NLS). A total of 31 (control), 21 (Hira siRNA), 11 (Hira siRNA and Hira mRNA co-injected), and 31 (H3.3 siRNA) zygotes were examined. P, paternal pronucleus; M, maternal pronucleus. Scale bar, 20 μ m. (e) Representative images of zygotes stained with anti-Tet3 antibody. A total of 25 (control), 14 (Hira siRNA) and 24 (H3.3 siRNA) zygotes were examined. Scale bar, 20 μ m. (f) Representative images of zygotes stained with anti-Ran antibody. A total of 23 (control), 33 (Hira siRNA) and 34 (H3.3 siRNA) zygotes were examined. Scale bar, 20 μ m. (g) Representative images of zygotes stained with mAb414. A total of 27 (control), 21 (Hira siRNA) and 46 (H3.3 siRNA) zygotes were examined. Scale bar, 20 μ m.



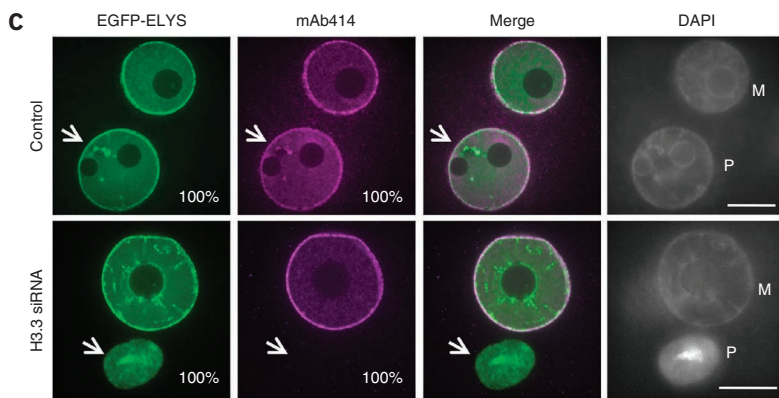
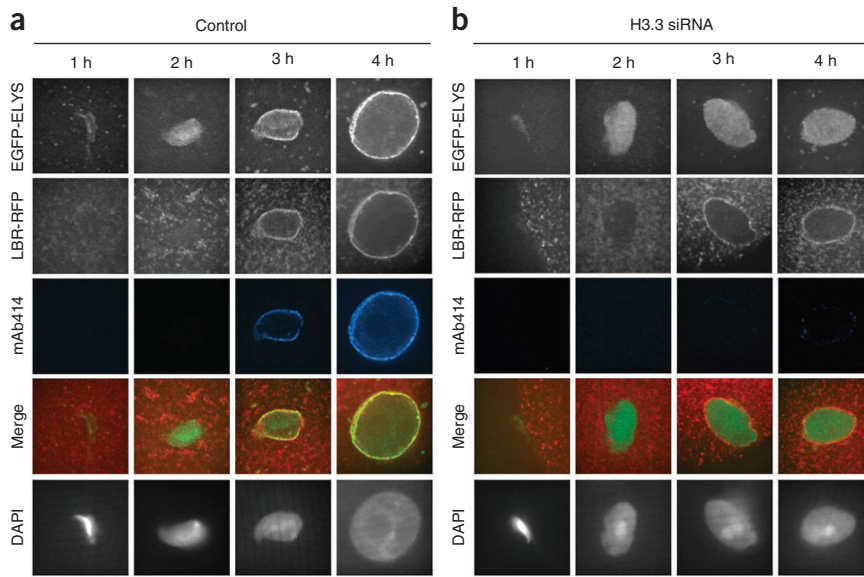


Figure 4 Loss of nucleosome assembly prevents the location of ELYS to the nuclear rim. **(a,b)** Representative images of the paternal DNA in control **(a)** and H3.3-depleted **(b)** zygotes stained with mAb414 (blue) and DAPI at the indicated times post fertilization. Merge shows EGFP (green) and RFP (red) channels. A total of 4 and 5 (1 h), 5 and 12 (2 h), 5 and 10 (3 h), and 7 and 12 (4 h) zygotes for control and H3.3-depleted zygotes, respectively, were examined. Scale bars, 10 μ m. **(c)** Representative images of zygotes stained with mAb414 (magenta) at 8 hpf. A total of 26 and 70 of control and H3.3-depleted zygotes, respectively, were examined. Percentages indicate zygotes showing the depicted phenotype. P, paternal pronucleus (indicated by arrows); M, maternal pronucleus. Scale bars, 20 μ m.

nuclear localization signal (NLS)¹⁸. Although EGFP-NLS, whose molecular weight is \sim 29 kDa, accumulated in both pronuclei of control zygotes, it failed to localize to the ND paternal pronuclei (**Fig. 3d**). We consistently found that nuclear lamin B1, whose assembly requires nuclear transport²⁴, failed to be assembled (**Fig. 3d**). Importantly, both defects were rescued by injection of Hira mRNA (**Fig. 3d**). In addition, the endogenous nuclear protein Tet3, normally localized exclusively in the paternal pronucleus²⁵, was no longer localized in ND pronuclei (**Fig. 3e**). Furthermore, the small GTPase Ran, a regulatory protein responsible for nuclear transport^{26,27}, did not accumulate (**Fig. 3f**). The absence of a nuclear-transport

system prompted us to examine whether the NPCs were correctly assembled. Immunostaining of NPCs with the monoclonal antibody mAb414 revealed that NPCs were not assembled around the ND paternal pronuclei, whereas they were readily detectable in the maternal

the ND pronucleus, we analyzed the assembly of NE components. Microinjection of mRNA encoding EGFP-tagged emerin or LBR, integral components of the inner NE²³, revealed that NEs surrounding ND paternal DNA were indeed visible (**Fig. 3a**). The NEs appeared to intrude into the 4',6-diamidino-2-phenylindole (DAPI)-stained DNA-containing regions, but we did not observe this in the maternal pronuclei or in both pronuclei of control zygotes (**Fig. 3a**). Detailed analysis by transmission electron microscopy (TEM) revealed that a double membrane surrounding the ND paternal DNA had formed (**Fig. 3b** and **Supplementary Fig. 4**). Consistently with the intrusion observed (**Fig. 3a**), TEM revealed invaginations of the inner membrane (**Fig. 3b**), which we did not observe in the control pronuclei. Despite the slight morphological difference, the NEs seemed to be completely sealed as 70-kDa dextrans were excluded from the ND pronuclei (**Fig. 3c**). Thus, the presence of sealed NEs suggests that nucleosome assembly is not required for NE formation.

We next asked whether the NE is functional for protein transport. To this end, we injected mRNA encoding EGFP fused to a classical

system prompted us to examine whether the NPCs were correctly assembled. Immunostaining of NPCs with the monoclonal antibody mAb414 revealed that NPCs were not assembled around the ND paternal pronuclei, whereas they were readily detectable in the maternal

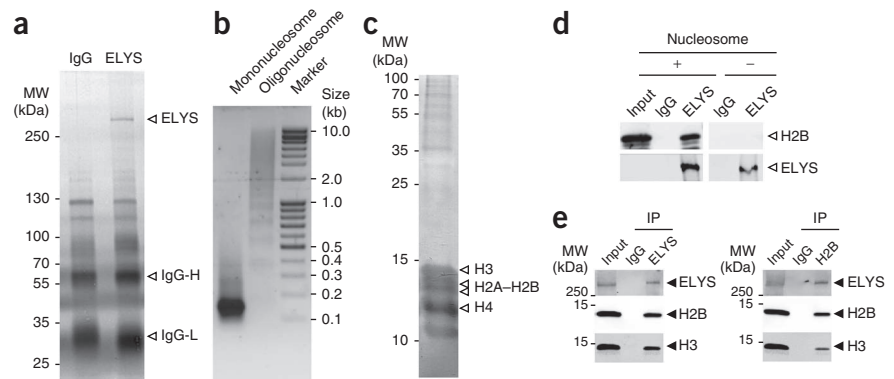


Figure 5 ELYS can interact with nucleosomes. **(a)** Silver-stained gel containing purified ELYS. Heavy (IgG-H) and light chains (IgG-L) of antibody are indicated at right. MW, molecular weight. **(b)** Ethidium bromide staining of DNA after phenol-chloroform extraction from the purified mono- or oligonucleosomes. **(c)** Coomassie brilliant blue-stained SDS-PAGE gel of purified mononucleosomes. H3, H2A–H2B and H4 are indicated. **(d)** *In vitro* interaction between purified ELYS and nucleosomes. + and – indicate presence and absence of nucleosomes, respectively. The full images are shown in **Supplementary Figure 7a,b**. **(e)** Coimmunoprecipitation of ELYS and histones from HEK293T cell extracts. Representative image from two independent experiments with similar results is shown. The full images are shown in **Supplementary Figure 7c–e**.

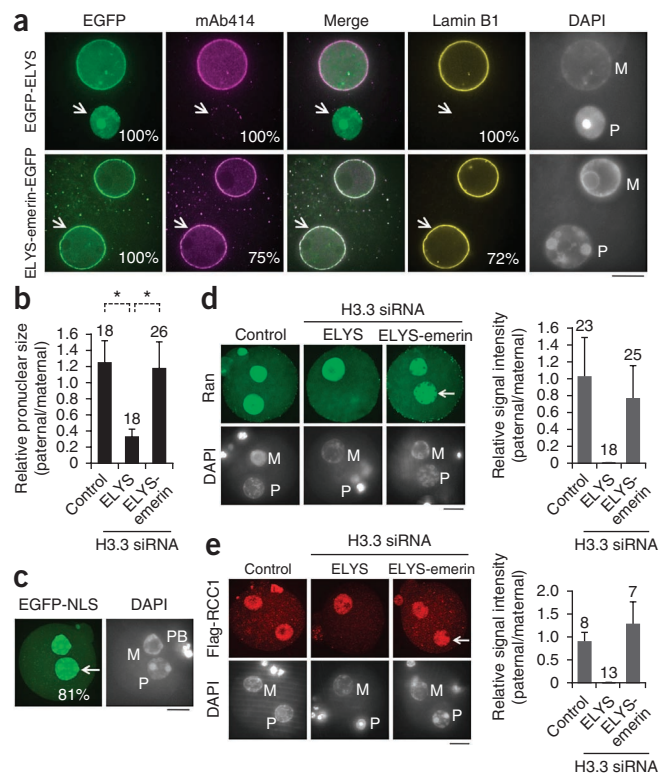
Figure 6 Forced nuclear-rim localization of ELYS results in functional NPC formation. (a) Representative images of H3.3-depleted zygotes stained with mAb414 (magenta), anti-lamin B1 antibody (yellow) and DAPI after EGFP-ELYS or ELYS-emerin-EGFP (green) mRNA injection at GV stage. A total of 30 (mAb414) or 40 (lamin B1) EGFP-ELYS and 16 (mAb414) or 36 (lamin B1) ELYS-emerin-EGFP zygotes were examined. Merge shows EGFP and mAb414 channels. Percentages indicate zygotes showing the depicted phenotype. P, paternal pronucleus (indicated by arrows); M, maternal pronucleus. Scale bar, 20 μ m. (b) Relative values of the area of pronuclei (paternal/maternal). The numbers of zygotes quantified in the experiments with biological triplicates are indicated above the bars. * $P < 0.01$ by two-tailed Student's t test; error bars, s.d. (c) Representative images of the rescued zygotes expressing EGFP-NLS. The arrow indicates the rescued paternal pronucleus. A total of 16 zygotes were examined. (d) Representative images of zygotes stained with anti-Ran antibody. Graph at right indicates relative values of the signal intensity (paternal/maternal). The numbers of zygotes examined are indicated above the bars. Error bars, s.d. (e) Representative images of zygotes stained with anti-Flag antibody. Flag-RCC1 mRNA was injected at GV stage. Graph at right indicates relative values of the signal intensity (paternal/maternal). The numbers of zygotes examined are indicated above the bars. Error bars, s.d.

pronuclei (Fig. 3g). Taken together, these results demonstrate that a NE devoid of NPCs is assembled in the ND paternal pronucleus.

Nucleosome loss prevents enrichment of ELYS to the nuclear rim

To understand the molecular basis by which the lack of nucleosome assembly prevents NPC assembly, we focused on ELYS for two reasons. First, it has been shown that ELYS is essential for the initial step of postmitotic NPC assembly^{23,28}. Second, ELYS-depleted *Xenopus* egg extracts are capable of assembling NE without NPCs^{29,30}, similarly to what we observed in ND paternal pronuclei (Fig. 3). To monitor the dynamics of ELYS during paternal pronuclear formation, we microinjected EGFP-ELYS mRNA. In control zygotes, ELYS was first evenly distributed along all decondensed sperm chromatin at 2 hpf (Fig. 4a) and became enriched at the rim of the chromatin mass at 3 hpf, concomitantly with the appearance of LBR-RFP (NE) and mAb414 (NPC) signals (Fig. 4a). In contrast, although ELYS localized to the decondensed ND paternal DNA at 2 hpf in H3.3-depleted zygotes, it failed to be enriched in the nuclear rim at 3–4 hpf (Fig. 4b). As a consequence, NPCs failed to be assembled, although NEs were assembled (Fig. 4b). In contrast to our observations for the paternal pronucleus, H3.3-depletion did not affect the dynamics of ELYS during maternal pronuclear formation, in which ELYS localizes to the surface of the maternal chromosome mass shortly after fertilization (Supplementary Fig. 5). The EGFP-ELYS distribution during maternal pronuclear formation is reminiscent of that in postmitotic somatic cells^{29,31}, thus suggesting that EGFP-tagged ELYS behaves similarly to endogenous ELYS. At 8 hpf, ELYS localized to the nuclear rim and also in the nuclear interior, with a dotted pattern in the maternal pronuclei of H3.3-depleted zygotes (Fig. 4c). This result is consistent with the ELYS distribution pattern previously observed in somatic cells³². In contrast, ELYS failed to localize to the nuclear rim of ND paternal pronuclei (Fig. 4c), thus suggesting that nucleosome assembly is a prerequisite for the nuclear-rim localization of ELYS.

To further confirm the above observation, we examined the localization of the Nup107–Nup160 complex, a building block of NPCs, whose recruitment to chromatin depends on ELYS^{28,29}. Microinjection of mRNA encoding Nup37, a component of the Nup107–Nup160 complex, fused to EGFP, revealed that Nup37 localized to the nuclear rim of control pronuclei, where it merged with the mAb414 signal, but it was not detected in the ND pronuclei (Supplementary Fig. 6a). Moreover, we found that POM121, a nuclear-pore integral membrane



protein whose localization also depends on ELYS *in vitro*³³, was undetectable in the ND pronuclei (Supplementary Fig. 6b). These results further demonstrate that ELYS fails to localize to the nuclear rim of the ND paternal pronucleus.

To gain insight into the mechanism by which nucleosome assembly is involved in the localization of ELYS in the nuclear rim, we asked whether ELYS could associate with nucleosomes. To this end, we purified ELYS from HEK293T cells, by using anti-ELYS antibody-coated beads (Fig. 5a), and also isolated mononucleosomes from HeLa cells (Fig. 5b,c). Incubation of the ELYS-bound beads and the control IgG beads, with or without mononucleosomes, and subsequent blotting with anti-H2B antibody demonstrated that ELYS associates with mononucleosomes (Fig. 5d and Supplementary Fig. 7). Furthermore, immunoprecipitation with anti-ELYS antibody from HEK293T cell protein extracts and subsequent blotting with anti-H2B and anti-H3 antibodies revealed that ELYS and nucleosomes interacted in the protein extracts (Fig. 5e and Supplementary Fig. 7). Consistently with this, anti-H2B antibody coprecipitated ELYS from the cell extracts. In combination with our observation that ELYS could not properly localize to the nuclear rim in the absence of nucleosomes (Fig. 4), these results suggest that ELYS-nucleosome interaction might contribute to nuclear-rim localization of ELYS.

Because it has been shown that Ran-GTP regulates ELYS-chromatin association *in vitro*³⁴ and that RNA interference-mediated depletion of Ran-system components causes defective localization of Mel-28, a *Caenorhabditis elegans* ortholog of mammalian ELYS³⁵, we examined whether the Ran-mediated protein transport system regulates the proper localization of ELYS in mouse zygotes. To disrupt the Ran system, we overexpressed dominant-negative forms of Ran (Ran^{Q69L} and Ran^{T24N})^{36,37}. We confirmed that Ran mutants and wild type (Ran^{WT}) were expressed at a similar level (Supplementary Fig. 8a) and that the expression of the mutants inhibited lamin B1 assembly and nuclear expansion (Supplementary Fig. 8b), thus indicating that

Figure 7 Core histones are largely absent in the rescued paternal pronucleus. **(a,b)** Representative images of zygotes stained with anti-H2A and anti-H2AX antibodies **(a)** or with anti-Flag antibody **(b)**. Flag-H2B mRNA was injected at GV stage. The arrows indicate the rescued paternal pronuclei. P, paternal pronucleus; M, maternal pronucleus; PB, polar body. Scale bars, 20 μ m. Graphs at right indicate relative values of the signal intensity (paternal/maternal). The numbers of zygotes examined in three independent experiments are indicated above the bars. * $P < 0.01$ by two-tailed Student's *t* test. Error bars, s.d.

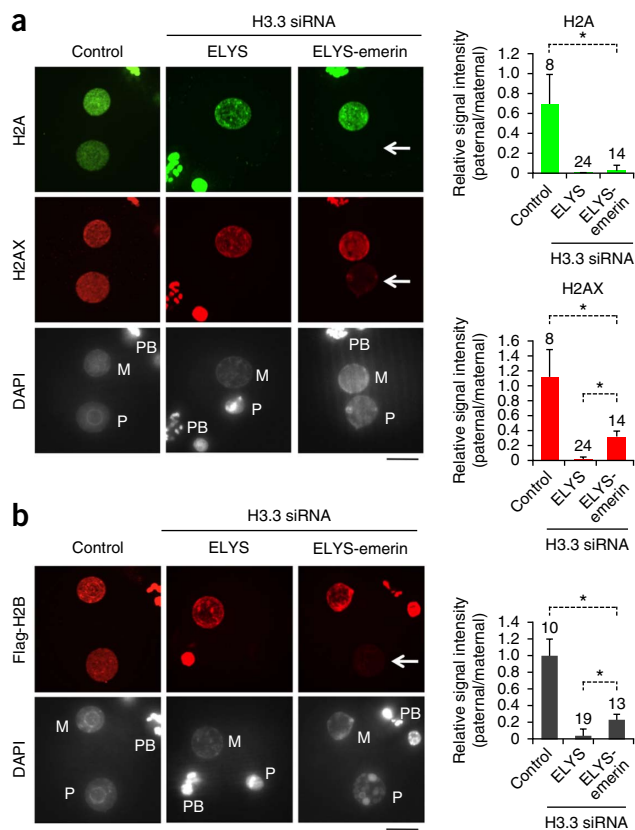
these mutants can efficiently block the Ran-mediated transport system. Co-injection of EGFP-ELYS mRNA with Ran mRNA revealed that ELYS localized to the surface of the maternal chromosome mass and the entire paternal chromatin in Ran^{WT} zygotes at 2 hpf and that this localization pattern did not change in the zygotes expressing the Ran mutants (**Supplementary Fig. 8c**). Importantly, the localization of ELYS in the nuclear rim of both pronuclei was also not affected by the Ran mutants at 8 hpf (**Supplementary Fig. 8d**). Notably, NPCs, marked by mAb414, could be assembled in zygotes expressing the Ran mutants, although we observed a substantial reduction of the signal in the Ran^{Q69L} mutant (**Supplementary Fig. 8d**). These results suggest that Ran-mediated nuclear transport is not responsible for the localization of ELYS to the nuclear rim in mouse zygotes.

Tethering ELYS to the NE of the ND nucleus rescues NPC assembly

To determine the causal relation between nuclear-rim localization of ELYS and NPC assembly, we asked whether the defect of NPC assembly in the ND paternal pronucleus could be rescued by tethering ELYS to the nuclear rim. To this end, we fused emerlin, an inner-NE protein localized in the nuclear rim of the ND pronucleus (**Fig. 3a**), to the 3' end of ELYS by generating a fusion construct, ELYS-emerin-EGFP. After microinjection of the mRNA into H3.3-depleted oocytes and subsequent meiotic maturation and fertilization, we confirmed that ELYS-emerin-EGFP protein indeed localized to the rim of the ND paternal pronuclei, whereas EGFP-ELYS localized only to the nuclear interior (**Fig. 6a**). Importantly, tethering ELYS to the nuclear rim rescued NPC assembly marked by mAb414 (**Fig. 6a**). Surprisingly, lamin B1 assembly as well as nuclear expansion was also rescued (**Fig. 6a,b**), thus suggesting recovery of the nuclear-transport system. Indeed, we observed EGFP-NLS accumulation in the rescued paternal pronuclei (**Fig. 6c**). Furthermore, the accumulation of both Ran and regulator of chromosome condensation 1 (RCC1) recovered (**Fig. 6d,e**). In contrast, immunostaining with anti-H2A and anti-H2AX antibodies (**Fig. 7a**) or microinjection of Flag-H2B mRNA followed by immunostaining (**Fig. 7b**) revealed that the rescued paternal pronuclei were still largely devoid of nucleosomes. Taken together, these data not only demonstrate that nucleosome assembly is upstream of nuclear-rim localization of ELYS and NPC assembly but also suggest that the defective localization of ELYS to the nuclear rim is the main cause of the defective NPC assembly observed in the ND paternal pronuclei.

DISCUSSION

In this study, we generated nucleosome-depleted (ND) paternal pronuclei *in vivo* in mouse zygotes by inhibiting maternal-histone incorporation into the paternal DNA. Phenotypic analyses of the ND pronuclei revealed that the loss of nucleosome assembly prevents the enrichment of ELYS to the nuclear rim and causes formation of the nonfunctional small pronucleus surrounded by a NE devoid of NPCs. The data presented here, in combination with previous studies, suggest a stepwise model for the formation of the paternal pronucleus in mouse zygotes (**Fig. 8**). After a sperm enters an egg, protamines are removed by undefined factors, the paternal DNA is decondensed



by nucleoplasmin 2 (ref. 38), and H3.3–H4 is deposited by HIRA. Protamine removal seems to be independent of histone deposition in mice (**Supplementary Fig. 2**), similarly to that in *Drosophila*³⁹ but not to that in *Xenopus*, in which nucleoplasmin is responsible for both the removal of protamine-like proteins and the deposition of maternal histones⁴⁰. Sperm DNA decondensation is also likely to be independent of histone deposition, because paternal DNA can be normally decondensed in the absence of maternal-histone deposition in H3.3-depleted zygotes (**Fig. 4b**). The exclusive targeting of HIRA to paternal DNA is independent of the presence of H3.3 (**Supplementary Fig. 3b**) and could be explained by the ability of HIRA to directly bind to naked DNA⁹, given that the paternal DNA, but not the maternal DNA, may transiently adopt a nucleosome-free state after protamine removal. Incorporation of H3.3–H4 appears to be a prerequisite for H2A–H2B deposition, because the H2A–H2B dimer is not incorporated in the absence of H3.3 or HIRA (**Fig. 2c,d**). During sperm DNA decondensation, ELYS becomes localized to the paternal chromatin (**Fig. 4a**). This initial localization of ELYS to chromatin is independent of *de novo* nucleosome assembly, because ELYS can localize to ND paternal DNA (**Fig. 4b**), possibly as mediated by its AT-hook motif with DNA-binding activity^{30,33}. During NE assembly, ELYS is enriched around the nuclear rim, and this requires preassembled nucleosomes (**Fig. 4a,b**). Whether the nuclear-rim localization of ELYS requires NE assembly remains to be determined. Enrichment of ELYS to the nuclear rim triggers the assembly of NPCs. This enables import of nuclear proteins, such as lamin B1 and Tet3, and expansion of the nuclear size via the Ran-mediated nuclear-transport system²¹ (**Fig. 3d–f**). However, a defect in *de novo* nucleosome assembly in the paternal pronucleus prevents the enrichment of ELYS to the nuclear rim but does not prevent the assembly of the NE. This leads to the formation of a NE devoid of NPCs (**Fig. 3g**), which in turn prevents nuclear import and nuclear expansion (**Fig. 3d–f**). Thus, we propose

Figure 8 Stepwise model depicting paternal pronuclear formation after fertilization. The left and right pathways indicate molecular steps of paternal pronuclear formation in wild-type zygotes and HIRA- or H3.3-depleted zygotes, respectively. Red dots indicate ELYS. Red nuclear membrane (NE) indicates functional NE-containing NPCs. Orange NE indicates nonfunctional NE lacking NPCs.

that HIRA-mediated *de novo* nucleosome assembly has a critical role in NPC assembly during paternal pronuclear formation (Fig. 8).

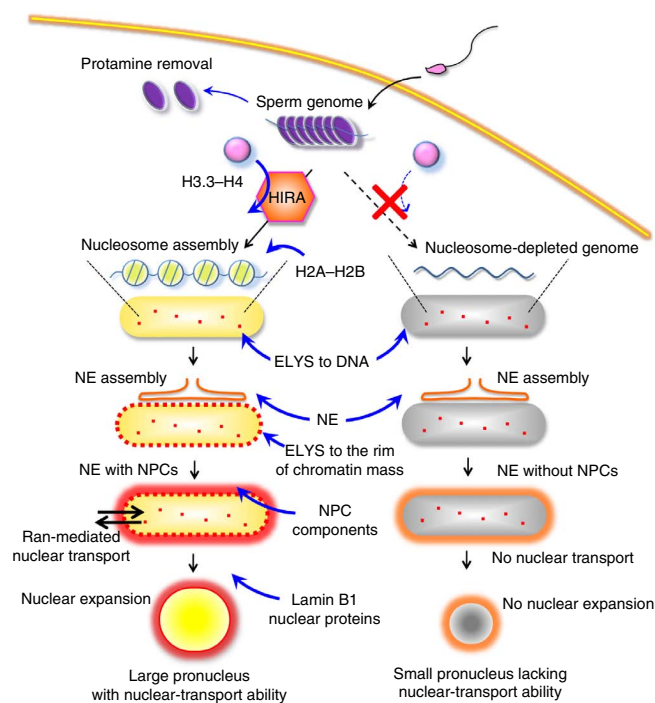
The *in vivo* zygote and the *in vitro* egg-extract system

Despite the great contribution of the *in vitro* *Xenopus* egg-extract system in defining many of the molecular events leading to the assembly of the NE and NPC, the role of nucleosomes in these processes could not be properly addressed because histones present in the extracts are spontaneously assembled onto the exogenous DNA, and this makes it difficult to distinguish the role of DNA and nucleosomes in the processes^{41,42}. Therefore, it has been unclear whether DNA or nucleosomes are required for the formation of functional NEs. In our study, we successfully generated nucleosome-free DNA *in vivo* and found that a NE without NPCs is formed in the absence of nucleosomes (Fig. 3). The presence of a sealed NE suggests that DNA may be sufficient, but nucleosome assembly is not required, for NE assembly. This finding is supported by previous studies demonstrating that inner-NE proteins including LBR, Man1 and Lap2 β can directly bind to a naked DNA *in vitro*⁴³ and that a protein-free DNA is more efficient for NE formation than a chromatinized DNA⁴⁴.

Proper localization of ELYS to the nuclear rim is required for NPC assembly (Fig. 4b,c). Although previous studies using *Xenopus* egg extracts reported that ELYS can bind to sperm chromatin that contains both DNA and nucleosomes *in vitro*^{29,30,33}, it has been unclear whether DNA or nucleosomes are responsible for the chromatin association of ELYS. The nuclear interior distribution of ELYS in the ND pronucleus suggests that, although ELYS might associate with DNA, such DNA-ELYS interaction is not sufficient for proper localization of ELYS to the nuclear rim and for subsequent recruitment of NPC components such as the Nup107–Nup160 complex (Supplementary Fig. 6). Once ELYS is artificially brought to the inner NE, functional NPCs can be assembled (Fig. 6), thus indicating that accumulation of ELYS at the nuclear rim is critical for initiating NPC assembly. We propose, on the basis of these observations and the demonstration that ELYS directly interacts with nucleosomes (Fig. 5), that nucleosomes might function as a scaffold for the accumulation of ELYS at the interface between chromatin and the NE. Future studies should reveal the molecular details of how ELYS accumulates at the nuclear rim in a nucleosome-dependent manner.

Potential mechanism regulating ELYS localization

How the location of ELYS is regulated is a fascinating question. Given that NE assembly and the localization of ELYS to the rim of the chromatin mass occur in a similar time frame during paternal pronuclear formation (Fig. 4a), it is possible that the contact between the NE and chromatin helps ELYS accumulate at the chromatin-NE interface. ELYS is integrated in NPCs at interphase and is believed to be oligomerized with other nucleoporins, including integral membrane proteins, to assemble an eight-fold-symmetrical structure^{23,45,46}. The integration of ELYS may lead to the apparent enrichment of ELYS at the nuclear rim. The important contribution of NE to the nuclear-rim localization of ELYS is supported by a study using *Xenopus* egg extracts, in which the absence of membranes prevented



the oligomerization of ELYS and the Nup107–Nup160 complex on the surface of the chromatin mass⁴⁷. However, it is also known that targeting of ELYS to the surface of the chromosome during anaphase of mitosis is independent of NE assembly, because it precedes the NE re-formation^{23,31,48}. This targeting is proposed to be achieved by DNA-binding activity, because the ELYS C-terminal domain contains an AT-hook motif with DNA-binding activity, which can mediate chromatin association *in vitro*^{30,33}. Thus, the mechanism of nuclear-rim localization at interphase may be different from that of chromosome-surface localization at anaphase. Owing to the highly compacted chromosome structure, ELYS's access to chromatin might be limited, thus trapping ELYS on the surface of the chromosome mass. In support of this notion, we found that ELYS localized to the entire paternal chromatin that did not form chromosome architecture after sperm DNA decondensation (Fig. 4a), while also localizing to the surface of the maternal chromosome mass at the same time (Supplementary Fig. 5). Subsequent enrichment of ELYS at the paternal nuclear rim might be caused by oligomerization of ELYS with other integral nucleoporins. It will be interesting to determine whether the contact of the NE is indeed required for the nuclear-rim localization of ELYS.

Implication in eukaryotic evolution

We speculate, on the basis of our finding that nucleosome assembly is a prerequisite for functional NE formation and the fact that prokaryotes have neither a NE nor nucleosomes and acquired both as they evolved into eukaryotes, that acquisition of nucleosome structures might precede acquisition of a functional NE during eukaryotic evolution. Although this hypothesis is difficult to prove, it is consistent with the fact that archaea have a tetrasome—a prototype of the octameric nucleosomes—but do not have a functional NE⁴⁹.

Additional discussion is in the **Supplementary Note**.

METHODS

Methods and any associated references are available in the [online version of the paper](#).

Note: Any Supplementary Information and Source Data files are available in the online version of the paper.

ACKNOWLEDGMENTS

We thank T. Haraguchi (Osaka University) and T. Kirchhausen (Harvard Medical School) for helpful discussion, F. Aoki (University of Tokyo) for the EGFP-NLS, Flag-H2B and Flag-H4 constructs, and I. Mattaj (European Molecular Biology Laboratory) and G.L. Xu (Chinese Academy of Sciences) for antibodies. We thank T. Haraguchi, G. German, S. Yamaguchi, S. Matoba and D. Cai for critical reading of the manuscript. This work was supported by US National Institutes of Health (U01DK089565 to Y.Z.). A.I. is supported as a research fellow for Research Abroad of the Japan Society for the Promotion of Science. Y.Z. is supported as an Investigator of the Howard Hughes Medical Institute.

AUTHOR CONTRIBUTIONS

A.I. and Y.Z. conceived the project, designed the experiments and wrote the manuscript; A.I. performed experiments and analyzed the data.

COMPETING FINANCIAL INTERESTS

The authors declare no competing financial interests.

Reprints and permissions information is available online at <http://www.nature.com/reprints/index.html>.

- Kornberg, R.D. & Lorch, Y. Twenty-five years of the nucleosome, fundamental particle of the eukaryote chromosome. *Cell* **98**, 285–294 (1999).
- Luger, K., Dechassa, M. & Tremethick, D. New insights into nucleosome and chromatin structure: an ordered state or a disordered affair? *Nat. Rev. Mol. Cell Biol.* **13**, 436–447 (2012).
- Burgess, R.J. & Zhang, Z. Histone chaperones in nucleosome assembly and human disease. *Nat. Struct. Mol. Biol.* **20**, 14–22 (2013).
- Margueron, R. & Reinberg, D. Chromatin structure and the inheritance of epigenetic information. *Nat. Rev. Genet.* **11**, 285–296 (2010).
- Marzluff, W.F., Gongidi, P., Woods, K., Jin, J. & Maltais, L. The human and mouse replication-dependent histone genes. *Genomics* **80**, 487–498 (2002).
- Rykowski, M.C., Wallis, J., Choe, J. & Grunstein, M. Histone H2B subtypes are dispensable during the yeast cell cycle. *Cell* **25**, 477–487 (1981).
- Drané, P., Ouararhni, K., Depaul, A., Shuaib, M. & Hamiche, A. The death-associated protein DAXX is a novel histone chaperone involved in the replication-independent deposition of H3.3. *Genes Dev.* **24**, 1253–1265 (2010).
- Goldberg, A.D. *et al.* Distinct factors control histone variant H3.3 localization at specific genomic regions. *Cell* **140**, 678–691 (2010).
- Ray-Gallet, D. *et al.* Dynamics of histone H3 deposition *in vivo* reveal a nucleosome gap-filling mechanism for H3.3 to maintain chromatin integrity. *Mol. Cell* **44**, e288–e301 (2011).
- Jenkins, T.G. & Carrell, D. Dynamic alterations in the paternal epigenetic landscape following fertilization. *Front. Genet.* **3**, 143 (2012).
- Nonchev, S. & Tsanev, R. Protamine-histone replacement and DNA replication in the male mouse pronucleus. *Mol. Reprod. Dev.* **25**, 72–76 (1990).
- van der Heijden, G.W. *et al.* Asymmetry in histone H3 variants and lysine methylation between paternal and maternal chromatin of the early mouse zygote. *Mech. Dev.* **122**, 1008–1022 (2005).
- Elsaesser, S.J., Goldberg, A.D. & Allis, C.D. New functions for an old variant: no substitute for histone H3.3. *Curr. Opin. Genet. Dev.* **20**, 110–117 (2010).
- Talbert, P.B. & Henikoff, S. Histone variants: ancient wrap artists of the epigenome. *Nat. Rev. Mol. Cell Biol.* **11**, 264–275 (2010).
- Akiyama, T., Suzuki, O., Matsuda, J. & Aoki, F. Dynamic replacement of histone h3 variants reprograms epigenetic marks in early mouse embryos. *PLoS Genet.* **7**, e1002279 (2011).
- Torres-Padilla, M.E., Bannister, A., Hurd, P., Kouzarides, T. & Zernicka-Goetz, M. Dynamic distribution of the replacement histone variant H3.3 in the mouse oocyte and preimplantation embryos. *Int. J. Dev. Biol.* **50**, 455–461 (2006).
- Loppin, B. *et al.* The histone H3.3 chaperone HIRA is essential for chromatin assembly in the male pronucleus. *Nature* **437**, 1386–1390 (2005).
- Inoue, A. & Aoki, F. Role of the nucleoplasmin 2 C-terminal domain in the formation of nucleolus-like bodies in mouse oocytes. *FASEB J.* **24**, 485–494 (2010).
- Smith, S. & Stillman, B. Stepwise assembly of chromatin during DNA replication *in vitro*. *EMBO J.* **10**, 971–980 (1991).
- Nashun, B., Yukawa, M., Liu, H., Akiyama, T. & Aoki, F. Changes in the nuclear deposition of histone H2A variants during pre-implantation development in mice. *Development* **137**, 3785–3794 (2010).
- D'Angelo, M.A., Anderson, D., Richard, E. & Hetzer, M. Nuclear pores form *de novo* from both sides of the nuclear envelope. *Science* **312**, 440–443 (2006).
- Webster, M., Witkin, K. & Cohen-Fix, O. Sizing up the nucleus: nuclear shape, size and nuclear-envelope assembly. *J. Cell Sci.* **122**, 1477–1486 (2009).
- Güttinger, S., Laurell, E. & Kutay, U. Orchestrating nuclear envelope disassembly and reassembly during mitosis. *Nat. Rev. Mol. Cell Biol.* **10**, 178–191 (2009).
- Newport, J.W., Wilson, K. & Dunphy, W. A lamin-independent pathway for nuclear envelope assembly. *J. Cell Biol.* **111**, 2247–2259 (1990).
- Gu, T.P. *et al.* The role of Tet3 DNA dioxygenase in epigenetic reprogramming by oocytes. *Nature* **477**, 606–610 (2011).
- Clarke, P.R. & Zhang, C. Ran GTPase: a master regulator of nuclear structure and function during the eukaryotic cell division cycle? *Trends Cell Biol.* **11**, 366–371 (2001).
- Quimby, B.B. & Dasso, M. The small GTPase Ran: interpreting the signs. *Curr. Opin. Cell Biol.* **15**, 338–344 (2003).
- Doucet, C.M., Talamas, J. & Hetzer, M. Cell cycle-dependent differences in nuclear pore complex assembly in metazoa. *Cell* **141**, 1030–1041 (2010).
- Franz, C. *et al.* MEL-28/ELYS is required for the recruitment of nucleoporins to chromatin and postmitotic nuclear pore complex assembly. *EMBO Rep.* **8**, 165–172 (2007).
- Gillespie, P.J., Khoudoli, G., Stewart, G., Swedlow, J. & Blow, J. ELYS/MEL-28 chromatin association coordinates nuclear pore complex assembly and replication licensing. *Curr. Biol.* **17**, 1657–1662 (2007).
- Galy, V., Askjaer, P., Franz, C., López-Iglesias, C. & Mattaj, I. MEL-28, a novel nuclear-envelope and kinetochore protein essential for zygotic nuclear-envelope assembly in *C. elegans*. *Curr. Biol.* **16**, 1748–1756 (2006).
- Bilokapic, S. & Schwartz, T. Structural and functional studies of the 252 kDa nucleoporin ELYS reveal distinct roles for its three tethered domains. *Structure* **21**, 572–580 (2013).
- Rasala, B.A., Ramos, C., Harel, A. & Forbes, D. Capture of AT-rich chromatin by ELYS recruits POM121 and NDC1 to initiate nuclear pore assembly. *Mol. Biol. Cell* **19**, 3982–3996 (2008).
- Lau, C.K. *et al.* Transportin regulates major mitotic assembly events: from spindle to nuclear pore assembly. *Mol. Biol. Cell* **20**, 4043–4058 (2009).
- Fernandez, A.G. & Piano, F. MEL-28 is downstream of the Ran cycle and is required for nuclear-envelope function and chromatin maintenance. *Curr. Biol.* **16**, 1757–1763 (2006).
- Dumont, J. *et al.* A centriole- and RanGTP-independent spindle assembly pathway in meiosis I of vertebrate oocytes. *J. Cell Biol.* **176**, 295–305 (2007).
- Hughes, M., Zhang, C., Avis, J., Hutchison, C. & Clarke, P. The role of the ran GTPase in nuclear assembly and DNA replication: characterisation of the effects of Ran mutants. *J. Cell Sci.* **111**, 3017–3026 (1998).
- Inoue, A., Ogushi, S., Saitou, M., Suzuki, M. & Aoki, F. Involvement of mouse nucleoplasmin 2 in the decondensation of sperm chromatin after fertilization. *Biol. Reprod.* **85**, 70–77 (2011).
- Bonnefoy, E., Orsi, G., Couble, P. & Loppin, B. The essential role of *Drosophila* HIRA for *de novo* assembly of paternal chromatin at fertilization. *PLoS Genet.* **3**, 1991–2006 (2007).
- Philpott, A. & Leno, G.H. Nucleoplasmin remodels sperm chromatin in *Xenopus* egg extracts. *Cell* **69**, 759–767 (1992).
- Forbes, D.J., Kirschner, M. & Newport, J. Spontaneous formation of nucleus-like structures around bacteriophage DNA microinjected into *Xenopus* eggs. *Cell* **34**, 13–23 (1983).
- Newport, J. Nuclear reconstitution *in vitro*: stages of assembly around protein-free DNA. *Cell* **48**, 205–217 (1987).
- Ulbert, S., Platani, M., Boue, S. & Mattaj, I. Direct membrane protein-DNA interactions required early in nuclear envelope assembly. *J. Cell Biol.* **173**, 469–476 (2006).
- Anderson, D.J. & Hetzer, M. Nuclear envelope formation by chromatin-mediated reorganization of the endoplasmic reticulum. *Nat. Cell Biol.* **9**, 1160–1166 (2007).
- Szymborska, A. *et al.* Nuclear pore scaffold structure analyzed by super-resolution microscopy and particle averaging. *Science* **341**, 655–658 (2013).
- D'Angelo, M.A. & Hetzer, M.W. Structure, dynamics and function of nuclear pore complexes. *Trends Cell Biol.* **18**, 456–466 (2008).
- Rotem, A. *et al.* Importin β regulates the seeding of chromatin with initiation sites for nuclear pore assembly. *Mol. Biol. Cell* **20**, 4031–4042 (2009).
- Imamoto, N. & Funakoshi, T. Nuclear pore dynamics during the cell cycle. *Curr. Opin. Cell Biol.* **24**, 453–459 (2012).
- Malik, H.S. & Henikoff, S. Phylogenomics of the nucleosome. *Nat. Struct. Biol.* **10**, 882–891 (2003).

ONLINE METHODS

Microinjection into MII-stage oocytes. All animal studies were performed in accordance with guidelines of the Institutional Animal Care and Use Committee at Harvard Medical School. MII-stage oocytes were collected from 3-week-old superovulated BDF1 females by injecting 5 I.U. of PMSG (Harbor, UCLA) and hCG (Millipore). The cumulus cells were removed by a short incubation in M2 medium containing 0.3 mg/ml hyaluronidase (Millipore), and oocytes were transferred into α -MEM medium (Life Technologies 12571-063) supplemented with 5% FBS. For microinjection, MII oocytes were transferred into M2 medium (Millipore) and injected with ~10 μ l of 50 ng/ μ l Flag-H3.3 mRNA with a Piezo impact-driven micromanipulator (Prime Tech Ltd., Ibaraki, Japan). After injection, oocytes were incubated in α -MEM for 3 h.

For *in vitro* fertilization (IVF), MII oocytes were transferred into HTF medium supplemented with 10 mg/ml bovine serum albumin (BSA; Sigma-Aldrich) and inseminated with activated spermatozoa obtained from the caudal epididymides of adult BDF1 male mice. Spermatozoa capacitation was attained by 1 h incubation in HTF medium. For analysis of preimplantation development, fertilized oocytes were cultured in KSOM (Millipore) in a humidified atmosphere of 5% CO₂/95% air at 37.8 °C.

Microinjection into GV-stage oocytes. Fully grown GV-stage oocytes were obtained from BDF1 mice (8–12 weeks old) 44–48 h after injection with 7.5 I.U. PMSG. The ovaries were removed and transferred to M2 medium containing 0.2 mM 3-isobutyl-1-methylxanthine (IBMX; Sigma-Aldrich). The ovarian follicles were punctured with a 27-gauge needle, and the cumulus cells were gently removed from the cumulus–oocyte complexes with a narrow-bore glass pipette. The oocytes were then transferred into α -MEM supplemented with 5% FBS, 10 ng/ml EGF, and IBMX.

One hour after collection of GV oocytes, they were injected with a mixture of 2 μ M each of the Stealth siRNA specific for H3f3a (Life Technologies, 5'-GC GAGAAUUGCUCAGGACUCAA-3') and Silencer Select siRNA specific for H3f3b (Life Technologies, s67336) or 4 μ M ON-TARGETplus nontargeting control siRNA 1 (control siRNA) (Dharmacon, D-001810-01-05) with a Piezo impact-driven micromanipulator. Twenty-four hours after injection, oocytes were transferred to IBMX-free α -MEM to induce meiotic maturation.

For expression of Flag-tagged histones, 50 ng/ μ l of Flag-H2B or 250 ng/ μ l of Flag-H4 mRNA was injected into the GV oocytes right before *in vitro* maturation. Similarly, 100 ng/ μ l of emerin-EGFP or 1,000 ng/ μ l of LBR-EGFP or LBR-mRFP1 mRNA was injected for detection of NE. For analysis of Flag-RCC1 or Nup37-EGFP localization, 0.1 ng/ μ l or 600 ng/ μ l of mRNA, respectively, was injected. EGFP-ELYS or ELYS-emerin-EGFP was injected at the concentration of 200 ng/ μ l. One hour after injection, they were transferred to IBMX-free α -MEM. After *in vitro* maturation for 16–18 h, MII oocytes were transferred into HTF medium and inseminated with capacitated sperm. EGFP-NLS mRNA (300 ng/ μ l) was injected into fertilized oocytes 4 h after insemination. 70-kDa dextran conjugated with Texas Red (Molecular Probes, 0.5 mg/ml) was injected 1 h before fixation.

For overexpression of Ran, 1,000 ng/ μ l Ran^{WT}-mRFP1, Ran^{T24N}-mRFP1, or Ran^{Q69L}-mRFP1 mixed with 200 ng/ μ l EGFP-ELYS mRNA was injected into GV oocytes. One hour after injection, they were transferred to IBMX-free α -MEM as described above.

Microinjection into growing oocytes and *in vitro* growth. The collection and culture of oocyte–granulosa cell complexes were performed as described previously with some modifications¹⁸. Oocyte–granulosa cell complexes were isolated from the ovaries of 12-day-old BDF1 females by mechanical dissection with 30-gauge needles. They were transferred into α -MEM with GlutaMax (Life Technologies, 32571-036) containing 5% FBS, 100 IU/L PMSG, 5 μ g/ml insulin (Sigma-Aldrich), 5 μ g/ml transferrin (Sigma-Aldrich), and 5 ng/ml sodium selenite (Sigma-Aldrich). Complexes meeting with all the morphological criteria described elsewhere³⁰ were culled, incubated for 1 h and then transferred into M2 medium for microinjection. 20 μ M of Silencer Select siRNA specific for Hira (Life Technologies, s67546) or 20 μ M control siRNA was injected into the cytoplasm of growing oocytes surrounded by granulosa layers with a Femtojet (Eppendorf) (Supplementary Fig. 1e). For rescue experiments, 160 ng/ μ l of Hira mRNA was co-injected with Hira siRNA. After microinjection, oocytes were transferred into the medium described above containing 2% polyvinylpyrrolidone (PVP, MW 360,000, Sigma-Aldrich)⁵¹. Five to seven complexes were cultured in a 50 μ l-drop

under mineral oil (Sigma-Aldrich). Half of the medium was exchanged for fresh medium every other day (Supplementary Fig. 1f).

After culturing for 12 d, the fully grown oocytes surrounded by cumulus cells were collected with a glass pipette and transferred into α -MEM supplemented with 5% FBS and 10 ng/ml EGF (Supplementary Fig. 1g). After meiotic maturation for 18 h, MII oocytes were transferred into HTF medium and inseminated with capacitated sperm.

Whole-mount immunostaining. Zygotes were fixed in 3.7% paraformaldehyde (PFA) in PBS (for anti-HIRA, anti-Tet3, anti-protamine 2 antibodies, and for EGFP-NLS) or 3.7% PFA/PBS containing 0.2% Triton X-100 (for the others) for 20 min and then washed with PBS containing 10 mg/ml BSA (PBS/BSA). After permeabilization with 0.5% Triton X-100 for 15 min (for the samples fixed without 0.2% Triton), zygotes were washed in PBS/BSA and treated with the following primary antibodies overnight at 4 °C: mouse anti-HIRA (1:100, Active Motif, 39557), mouse anti-Flag M2 (1:200, Sigma-Aldrich, F3165), rabbit anti-Flag (1:2,000, Sigma-Aldrich, F7425), goat anti-lamin B1 (1:500, Santa Cruz Biotechnology, sc-6217), mouse anti-H2A²⁰ (1:2,000, MBL, D210-3), rabbit anti-H2AX²⁰ (1:2,000, Abcam, ab11175), mouse anti-protamine 2 (1:100, Briar Patch Biosciences), rabbit anti-Tet3 (ref. 25; 1:4,000, a gift from G.L. Xu), mAb414 (1:2,000, Abcam, ab24609), rabbit anti-POM121 (1:1,000, GeneTex, 102128) or mouse anti-Ran (1:10,000, BD transduction laboratories, 610340). Validation of the antibodies for mouse antigens can be found on the manufacturer's websites. When using anti-Tet3 antibody, zygotes were incubated with primary-antibody solution for 2 h at room temperature. After washing with PBS/BSA for 30 min, samples were incubated with a 1:250 dilution of fluorescein isothiocyanate-conjugated anti-mouse IgG (Jackson Immuno-Research), Alexa Fluor 568 donkey anti-rabbit IgG (Life Technologies), Alexa Fluor 568 donkey anti-mouse IgG (Life Technologies), Alexa Fluor 647 donkey anti-mouse IgG (Life Technologies), and/or Alexa Fluor 647 donkey anti-goat IgG (Life Technologies) for 1 h. The oocytes were then mounted on a glass slide in Vectashield anti-bleaching solution with 4',6-diamidino-2-phenylindole (DAPI) (Vector Laboratories). Fluorescence was detected under a laser-scanning confocal microscope with a spinning disk (CSU-10, Yokogawa) and an EM-CCD camera (ImagEM, Hamamatsu). All images were acquired and analyzed with Axiovision (Carl Zeiss).

The fluorescence signal intensity was quantified with Axiovision. Briefly, the signal intensity within each parental pronucleus was determined, and the cytoplasmic signal was subtracted as background. Then, the relative intensity of the paternal and maternal signal was calculated. The area of pronuclei was also quantified with Axiovision.

Immunostaining for surface spread. Surface-spread samples for fertilized oocytes and sperm were prepared as described previously⁵². Briefly, fertilized oocytes with zona pellucida removed by treatment with acidic Tyrode's solution (Sigma-Aldrich) were put on a glass slide dipped in a solution of 1% PFA in DW, pH 9.2, containing 0.15% Triton X-100 and 3 mM dithiothreitol. After fixing overnight in a humid chamber, the slide was washed in 0.4% Photoflo (Kodak) in DW and dried for 30 min at room temperature. The samples were washed with 0.1% Tween-20/PBS, treated with 0.5% Triton X-100 for 15 min, and then incubated with rabbit anti-H2AX (1:2,000, Abcam, ab11175), mouse anti-protamine 2 (1:100, Briar Patch Biosciences), and/or human anti-Crest⁵³ antibodies (1:500, Antibodies Inc. 15-235) overnight. After washing with PBS/BSA for 30 min, samples were incubated with Alexa Fluor 568 donkey anti-rabbit IgG and Alexa Fluor 647 donkey anti-human IgG (Life Technologies) for 1 h.

Reverse transcription and real-time PCR analysis. RNA extraction and reverse transcription were performed with the SuperScript III CellsDirect cDNA Synthesis Kit (Life Technologies) according to the manufacturer's instructions. Real-time quantitative PCR reactions were performed on an ABI Vii7 real-time PCR detection system (Applied Biosystems) with SYBR Green (Applied Biosystems). Relative gene expression levels were analyzed with comparative Ct methods, where Ct is the threshold cycle number, and normalized to GAPDH. Primer sequences are as follows: Gapdh-F, 5'-CATGGCCTTCCGTGTTCCCTA-3'; Gapdh-R, 5'-GC CTGCTTACCACCTTCTT-3'; Hira-F, 5'-AAGGAGGCCATGTGTCTGTC-3'; Hira-R, 5'-GTCTCCCACTCCTTCCCTTC-3'; H3f3a-F, 5'-GTGGTAAA GCACCCAGGAAA-3'; H3f3a-R, 5'-TGCGGATCAGAAGTTCAGTG-3'; H3f3b-F, 5'-CTGCCATTCCAGAGATTGGT-3'; H3f3b-R, 5'-GGGCATGAT

GGTACTCTCT-3'. For multicopy histone genes, primers were designed in common sequences among all (H2B, H3.1, and H3.2)¹⁵ or most (H4) of genes. H2B-F, 5'-GCCGCAAGGAGACTACTC-3'; H2B-R, 5'-CGTTGTGTGTAATGCGCCAG-3'; H3.1-F, 5'-TGCAGGAGGCCTGTGA-3'; H3.1-R, 5'-TGATGTCCTTGGGCATG-3'; H3.2-F, 5'-TGCAGGAGGCAGCA-3'; H3.2-R, 5'-TGGATGTCCTTGGGCATG-3'; H4-F, 5'-AAGCGCATCTCCGGCCTCAT-3'; H4-R, 5'-GTCTTGCCTTGGCGTGCTC-3'.

Plasmid construction and mRNA preparation. To make the Flag-H3.3 construct, H3.3B (H3F3B) gene was amplified from pcDNA3.1-H3.3-EGFP-poly(A)83 plasmid⁵⁴ and cloned into pcDNA3.1-Flag-poly(A)83 plasmid, which was produced in this study. The H3.3 gene was inserted between the Flag tag and the poly(A). Hira cDNA was amplified from mouse ES-cell cDNA and cloned into the pcDNA3.1-poly(A)83 plasmid. Eight silent mutations were introduced into the siRNA 19-nucleotide targeting sequence with the PrimeSTAR mutagenesis basal kit (TAKARA). Primers for mutagenesis are as follows. 5'-GacaGgtcacTcaAGGTATGGAGGACGCTG-3' and 5'-CTTgAgtgacCtgcATCAGCTTGA GAGCA-3'.

To create the emerin-EGFP, LBR-EGFP, and LBR-mRFP1 constructs, the full-length mouse emerin gene or N-terminal domain of LBR⁵⁵ was amplified from mouse ES-cell cDNA and cloned into the pcDNA3.1-EGFP-poly(A)83 vector or pcDNA3.1-mRFP1-poly(A)83 plasmid⁵⁴. The emerin or LBR gene was inserted at the 5' end of EGFP. Similarly, full-length mouse ELYS cDNA was amplified and cloned into pcDNA3.1-EGFP-poly(A)83 to make an EGFP-ELYS construct. The ELYS gene was inserted into the 5' end of emerin-EGFP to make the ELYS-emerin-EGFP construct with the In-fusion HD cloning Kit (Clontech). Full-length mouse Ran cDNA was amplified from mouse ES-cell cDNA and cloned into pcDNA3.1-mRFP1-poly(A)83 plasmid to make a Ran^{WT}-mRFP1 construct. Point mutations for T24N and Q69L in the Ran gene were introduced with the PrimeSTAR mutagenesis basal kit. All constructs were verified by DNA sequencing.

mRNA was synthesized from linearized constructs by *in vitro* transcription with a mMESSAGE mMACHINE T7 or Sp6 Kit (Life Technologies) or mMES-SAGE mMACHINE T7 Ultra Kit (Life Technologies) according to the manufacturer's instructions. The synthesized mRNA was purified by lithium chloride precipitation and diluted with nuclease-free water.

Transmission electron microscopy. Sample preparation was performed by following the protocol of the Harvard Medical School EM facility. Briefly, zygotes were fixed overnight at 4 °C in 2.5% glutaraldehyde, 1.25% paraformaldehyde and 0.03% picric acid in 0.1 M sodium cacodylate buffer, pH 7.4. Samples were washed in 0.1 M cacodylate buffer, fixed with 1% osmium tetroxide (OsO₄)/1.5% potassium ferrocyanide (K₄[Fe(CN)₆]) for 2 h, washed in water three times and incubated in 1% aqueous uranyl acetate for 1 h. This was followed by two washes in water and subsequent dehydration in grades of alcohol (10 min each with 50%, 70%, 90%; 2 × 10 min with 100%). The samples were then put in propylene oxide for 1 h and infiltrated overnight in a 1:1 mixture of propylene oxide and Spurr's resin (EMS). On the following day, the samples were embedded in Spurr's and polymerized at 60 °C for 48 h.

Ultra-thin sections (about 60 nm) were cut on a Reichert Ultracut-S microtome, picked up on to copper grids, stained with lead citrate and examined in a JEOL 1200EX transmission electron microscope. Images were recorded with an AMT 2,000 CCD camera.

Immunoprecipitation. The cell lysate was prepared as described previously with some modifications⁵⁶. 1 × 10⁷ HEK293T cells were lysed with 70 μl of high-salt buffer (10 mM Tris-HCl, pH 7.4, 400 mM NaCl, 1% Triton X-100, 2 mM EGTA, 1 mM MgCl₂, 1 mM DTT, and protease-inhibitor cocktail EDTA-free (Roche 05892791001) containing benzonase nuclease (1:500, Millipore)) for 30 min at 4 °C. The sample was then sonicated briefly and centrifuged at 15,000 r.p.m. for 15 min. The supernatant was diluted with 190 μl of nonsalt buffer (10 mM Tris-HCl, pH 7.4, 2 mM EDTA, 1 mM DTT, and protease-inhibitor cocktail (Roche 11697498001)). After centrifugation at 15,000 r.p.m. for 15 min, the supernatant was incubated for 1 h at 4 °C with Dynabeads Protein A (Life Technologies) bound with 2 μg of rabbit anti-ELYS²⁹ (a gift from I. Mattaj), rabbit anti-H2B antibody (Abcam, ab1790; validation on the manufacturer's website), or rabbit IgG (Santa Cruz, sc-2027). After five washes with mixed buffer (high-salt

buffer/nonsalt buffer 1: 2.75), the proteins were eluted with SDS sample buffer. Five percent of the cell extract was loaded as the input. Twenty-nine percent of the precipitate was loaded for blotting with histone antibodies. Seven or 29 percent of the precipitate by ELYS- or H2B-specific antibody, respectively, was loaded for blotting with ELYS antibody.

Immunoblotting. For the analysis of immunoprecipitation, the proteins were separated by SDS-PAGE on 5% or 15% polyacrylamide gel and electrically transferred to nitrocellulose membrane (Bio-Rad). The membranes were blocked for 60 min at room temperature in Odyssey blocking buffer (LI-COR Biosciences). They were then incubated with rabbit anti-ELYS²⁹ (1:2,500) or rabbit anti-H2B (1:20,000, Abcam ab1790) and mouse anti-H3 (1:1,000, Millipore, 05-499) antibodies (validation on the manufacturers' websites) in Odyssey blocking buffer overnight at 4 °C. After washing with Tris-buffered saline containing 0.1% Tween-20 (TBST), the membranes were incubated with IRDye 800CW goat anti-mouse or/and IRDye 680RD goat anti-rabbit secondary antibody (1:5,000, LI-COR Biosciences) in TBS-T containing 0.5% BSA for 1 h at room temperature. The membranes were washed in TBS-T, and the fluorescence signal was detected with a LI-COR Odyssey Imager (LI-COR Biosciences). The original images of blots can be found in **Supplementary Figure 7a,b**.

For the analysis of Ran expression, MII oocytes were collected into 1× SDS sample buffer and heated at 95 °C for 5 min. The proteins were separated by SDS-PAGE on a 10% polyacrylamide gel and transferred to nitrocellulose membrane. The membranes were blocked in TBS-T containing 5% BSA and then incubated with mouse anti-Ran (1:2,000, BD transduction laboratories, 610340) or mouse anti- α -tubulin (1:4,000, Sigma-Aldrich, T6199) antibodies (validation on the manufacturers' websites) in TBS-T/1% BSA overnight at 4 °C.

In vitro binding assay. Mononucleosomes were purified from HeLa cells as described previously⁵⁷. The purification of mononucleosomes was confirmed by Coomassie brilliant blue staining following SDS-PAGE and by ethidium bromide staining following phenol-chloroform extraction of DNA.

For purification of ELYS, rabbit anti-ELYS antibody or rabbit IgG was cross-linked with Dynabeads Protein A by treatment with 20 mM dimethyl pime-limide (Sigma-Aldrich) in 200 mM sodium borate, pH 9.0, for 30 min at room temperature. The cross-linked beads were incubated with HEK293T cell extracts prepared as described above. After pulldown of ELYS, the beads were washed four times with 1 M NaCl for 5 min each to remove most binding proteins. For checking the quality of protein purification, a small aliquot of beads was boiled in SDS sample buffer, the proteins were separated by 7% Next gel (Amresco), and the gel was silver stained (Pierce). The rest of the beads were then washed with the mixed buffer described above and incubated with the mixed buffer containing mononucleosomes for 30 min at 4 °C. After three washes with the mixed buffer, the proteins were eluted with SDS sample buffer. Ten percent of the nucleosome solution was loaded as the input. Seventeen or 33 percent of the precipitate was loaded for blotting with anti-ELYS or anti-H2B antibody, respectively. The original images of blots can be found in **Supplementary Fig. 7c-e**.

Statistical analysis. Data were analyzed by two-tailed Student's *t* test. A value of *P* < 0.01 was considered statistically significant.

- Pesty, A., Miyara, F., Debey, P., Lefevre, B. & Poirot, C. Multiparameter assessment of mouse oogenesis during follicular growth *in vitro*. *Mol. Hum. Reprod.* **13**, 3–9 (2007).
- Hirao, Y. Isolation of ovarian components essential for growth and development of mammalian oocytes *in vitro*. *J. Reprod. Dev.* **58**, 167–174 (2012).
- Yamaguchi, S. *et al.* Dynamics of 5-methylcytosine and 5-hydroxymethylcytosine during germ cell reprogramming. *Cell Res.* **23**, 329–339 (2013).
- Ooga, M. *et al.* Changes in H3K79 methylation during preimplantation development in mice. *Biol. Reprod.* **78**, 413–424 (2008).
- Okada, Y., Yamagata, K., Hong, K., Wakayama, T. & Zhang, Y. A role for the elongator complex in zygotic paternal genome demethylation. *Nature* **463**, 554–558 (2010).
- Ellenberg, J. *et al.* Nuclear membrane dynamics and reassembly in living cells: targeting of an inner nuclear membrane protein in interphase and mitosis. *J. Cell Biol.* **138**, 1193–1206 (1997).
- Clever, M., Funakoshi, T., Mimura, Y., Takagi, M. & Imamoto, N. The nucleoporin ELYS/Mel28 regulates nuclear envelope subdomain formation in HeLa cells. *Nucleus* **3**, 187–199 (2012).
- Fang, J., Wang, H. & Zhang, Y. Purification of histone methyltransferases from HeLa cells. *Methods Enzymol.* **377**, 213–226 (2004).